Journal of Alloys and Compounds 509 (2011) 9419–9424

Contents lists available at ScienceDirect

Journal of Alloys and Compounds

journal homepage: www.elsevier.com/locate/jallcom

Microstructural and mechanical properties of Al–Mg/Al_2O_3 nanocomposite prepared by mechanical alloying

J. Safari [a,*], G.H. Akbari [a,b], A. Shahbazkhan [c], M. Delshad Chermahini [d]

[a] Department of Material Science and Engineering, Shahid Bahonar University of Kerman, P.O. Box No. 76135-133, Kerman, Iran
[b] Research Center for Mineral Industries, Shahid Bahonar University of Kerman, P.O. Box No. 76135-133, Kerman, Iran
[c] Islamic Azad University, Saveh Branch, Saveh, Iran
[d] Materials and Energy Research Center, Karaj, Iran

ARTICLE INFO

Article history:
Received 30 May 2011
Received in revised form 18 July 2011
Accepted 20 July 2011
Available online 27 July 2011

Keywords:
Scanning electron microscopy
X-ray diffraction
Al–Mg matrix nanocomposite
Mechanical alloying
Particle size

ABSTRACT

The effect of milling time on the microstructure and mechanical properties of Al and Al–10 wt.% Mg matrix nanocomposites reinforced with 5 wt.% Al_2O_3 during mechanical alloying was investigated. Steady-state situation was occurred in Al–10Mg/5Al_2O_3 nanocomposite after 20 h, due to solution of Mg into Al matrix, while the situation was not observed in Al/5Al_2O_3 nanocomposite at the same time. For the binary Al–Mg matrix, after 10 h, the predominant phase was an Al–Mg solid solution with an average crystallite size 34 nm. Up to 10 h, the lattice strain increased to about 0.4 and 0.66% for Al and Al–Mg matrix, respectively. The increasing of lattice parameter due to dissolution of Mg atom into Al lattice during milling was significant. By milling for 10 h the dramatic increase in microhardness (155 HV) for Al–Mg matrix nanocomposite was caused by grain refinement and solid solution formation. From 10 to 20 h, slower rate of increasing in microhardness may be attributed to the completion of alloying process, and dynamic and static recovery of powders.

1. Introduction

It is established that during mechanical alloying a solid state reaction takes place between the fresh powder surfaces of the reactant materials at room temperature. Consequently, it can be useful to produce alloys and compounds that are difficult and impossible to be obtained by conventional melting and casting techniques [1,2].

Al-based metal matrix composites, which possess high strength, high hardness, high-specific elastic modulus, etc., are being widely used in the aerospace and automobile industries [3]. Also, the addition of Cu, Mg and Si into Al matrix improves the mechanical properties caused by solid solution and age hardening [3]. Al–Mg alloys because of their high specific strength (strength to weight ratio) are used as matrix in Al-based nanocomposites [4,5]. Mechanical alloying has been used previously for the preparation of a range of Al–Mg alloys with bulk Mg concentrations varying from 3 to 70 at.% [4–12]. The equilibrium solid solubility of Mg in Al at room temperature is only about 1 at.% [13], indeed, the solubility of Mg in aluminum has been increased substantially by the mechanical alloying process [6–10].

Reinforcing of ductile Al matrix with hard particles such as oxides provides a suitable combination of the properties of both phases which, in turn, results in an improvement of physical and mechanical properties of composites [14–17]. Uniform dispersion of the fine reinforcements and a fine grain size of the matrix contribute to improve the mechanical properties of the composite [16].

Therefore, the objective of present work is the investigation of effect of milling time on morphological, microstructural and microhardness changes of Al/5 wt.% Al_2O_3 and Al–10 wt.% Mg/5 wt.% Al_2O_3 powder mixtures during the mechanical alloying process which has less been researched. In comparison with other work in this area, Al–Mg alloy instead of pure Al was used as matrix.

2. Materials and experimental procedures

Al (99%, <23 μm), Mg (99%, <136 μm) and Al_2O_3 (<135 μm) powders were mechanically alloyed under argon atmosphere to form Al–*x*Mg/5 wt.% Al_2O_3 (x = 0, 10 wt.%) composites in a Fritsch planetary ball mill, while confined in sealed 250 ml steel containers rotated at 250 rpm for a variety of milling times (2, 5, 10, 15 and 20 h). The container was loaded with a blend of balls (ϕ = 10 mm, mass = 4.14 g and ϕ = 20 mm, mass = 32.12 g). The total weight of the powder was about 20 g and the ball to powder mass ratio was about 20:1. Stearic acid (2 wt.%) was used as the process control agent to prevent excessive cold welding of powder particles.

Milled powder samples at different stages of milling were investigated by Cam Scan MV2300 SEM. Average particles size of powders at each stage was determined by tangential method using SEM micrographs.

X-ray diffraction measurements were carried out in a *Philips X'Pert High Score* diffractometer using Cu K_α (λ = 1.5405 Å) radiation over 20–140° 2θ. To adjust the

* Corresponding author.
E-mail address: safari.jam@gmail.com (J. Safari).

0925-8388/$ – see front matter © 2011 Published by Elsevier B.V.
doi:10.1016/j.jallcom.2011.07.061

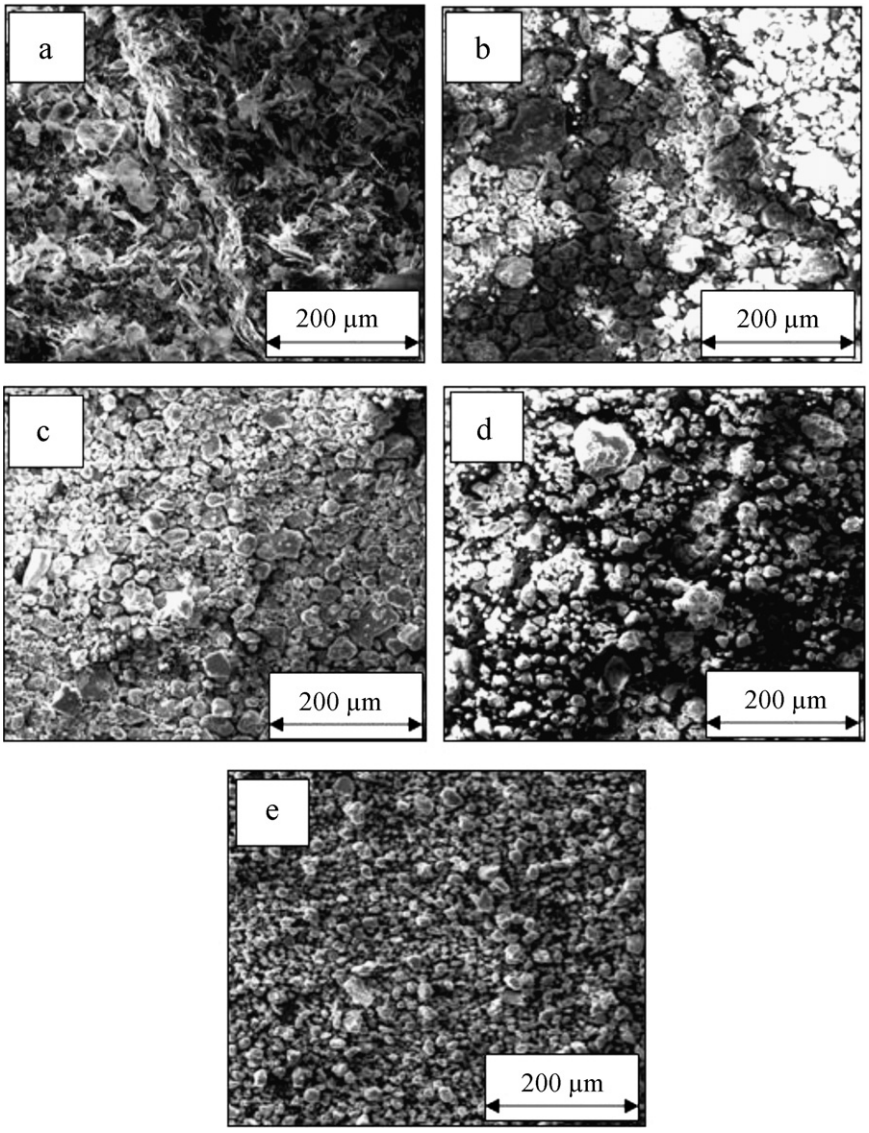

Fig. 1. SEM micrographs of Al–10Mg/5Al_2O_3 powders milled for different times: (a) 2 h, (b) 5 h, (c) 10 h, (d) 15 h and (e) 20 h.

shift of zero angle, the silicon crystal was used as a standard sample. The crystallite size and lattice strain were estimated using the Williamson–Hall method [18]:

$$\beta_s \cos\theta = \frac{K\lambda}{d} + 2\varepsilon \sin\theta \quad (1)$$

where β_s is the full-width at half-maximum of the diffraction peak, θ is the diffraction angle, λ is the X-ray wavelength, d is the crystallite size, and ε is the lattice strain. β_s can be given as:

$$\beta_s^2 = \beta_e^2 - \beta_i^2 \quad (2)$$

where β_i is the width at half-maximum of the Si powder peaks used for calibration and β_e is the evaluated width.

Thus, it is clear that when we plot $\beta_s \cos\theta$ against $\sin\theta$ we get a straight line with slope (ε) and intercept $K\lambda/d$. The crystallite size (d) can be calculated from $K\lambda/d$ (K and λ are determinate) and lattice strain is slop line (ε) [19].

The hardness of powders was determined by microhardness measurements using a Vickers indenter at a load of 250 milli-Newton and dwell time of 5 s. For measurement of microhardness, the powder mixtures were cold pressed under 25 MPa. Prior to indentation, the surfaces of samples were polished using a sequence of increasing grit sandpaper followed by a series of diamond pastes.

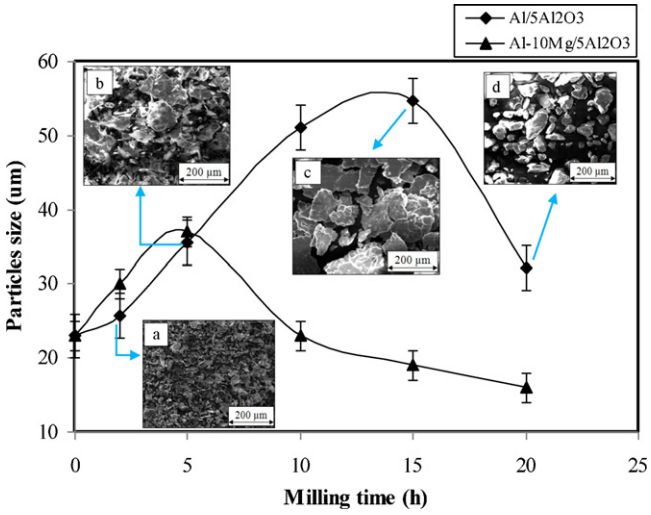

Fig. 2. Variation of particles size as a function of milling time for Al/5Al_2O_3 and Al–10Mg/5Al_2O_3 powder mixtures.

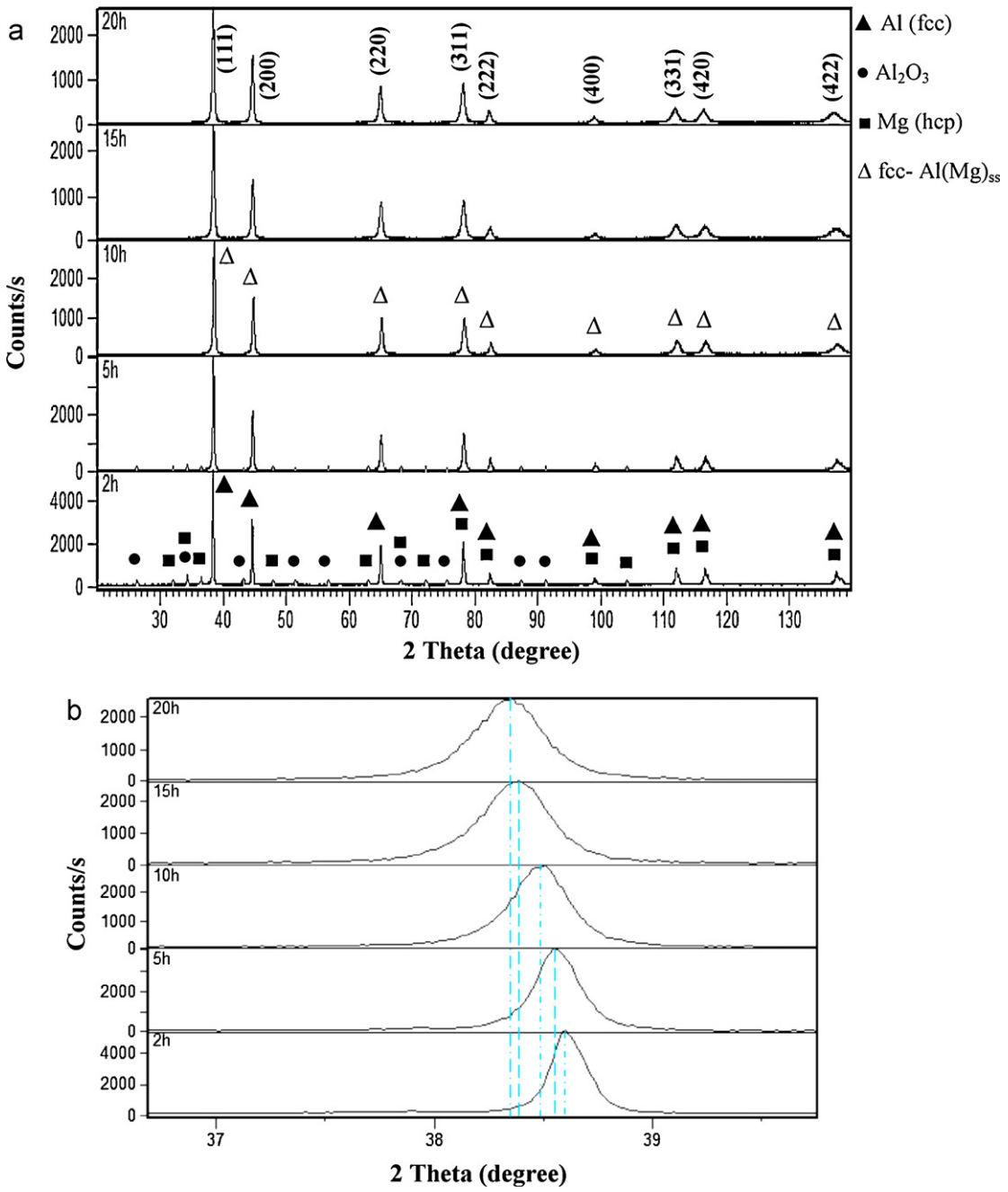

Fig. 3. X-ray diffraction patterns of Al–10Mg/5Al_2O_3 powder mixtures for different milling times.

3. Results and discussion

3.1. Morphology

Fig. 1(a–e) shows SEM micrographs of Al–10Mg/5Al_2O_3 nanocomposite powders mechanically alloyed for different milling times. In the early stages of milling (from 2 to 5 h), the powders are still soft and cold welding predominates. Consequently, the particles size increases (Fig. 1(b)). Particles shape has become flattened due to cold working effects during milling. As shown in Fig. 2 the maximum average particle size (37 μm) is obtained after 5 h. Fig. 1(c) illustrates that after 10 h of milling, particles have become more rounded in shapes and finer in average size. It suggests that predominant processes at this stage are cold working and fracturing with probably some recovery. Powder particles after 15 h seem equiaxed with almost the same size, but some coarse particles still remain (Fig. 1(d)). Eventually, when the milling time increased to 20 h (Fig. 1(e)) a balance is established between the cold welding and fracturing events and a steady-state situation is obtained. It means that the distribution of Al_2O_3 particles in the Al–Mg matrix is very uniform at this stage [16]. Also the average particles size of powder after 20 h milling is about 15 μm.

Also Fig. 2 shows for Al/5Al_2O_3 composite up to 15 h flattening and coarsening trends are observed and after 20 h, particles become finer and changing their shapes from flatten to almost equiaxed shapes but a steep reduction trend in particles size is still observed.

The cold worked structure of Al matrix with high dislocation density provides suitable conditions for diffusion of bigger Mg atoms (Mg atoms have a larger atomic radius than Al atoms) along dislocation lines into Al lattice [6]. Additionally, the decreased

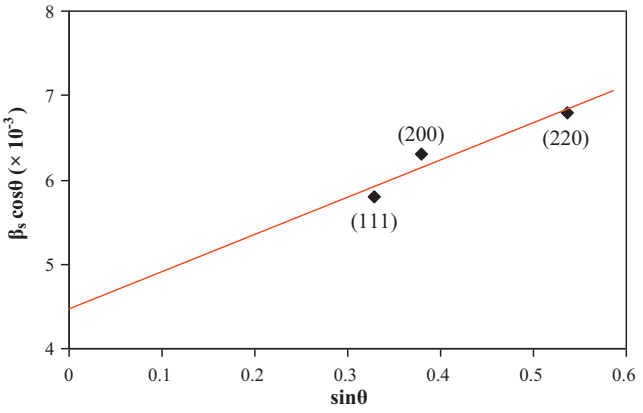

Fig. 4. Plot of $\beta_s \cos\theta$ versus $\sin\theta$ for Al–10Mg/5Al_2O_3 system milled to 20 h.

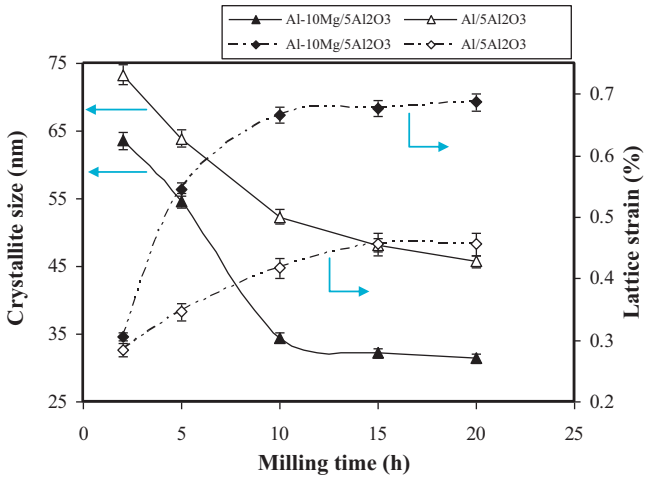

Fig. 5. Evolution of crystallite size and lattice strain for Al/5Al_2O_3 and Al–10Mg/5Al_2O_3 powder mixtures on several milling times.

particle size during milling reduces the diffusion distances between particles and facilitates diffusion. Diffusion is further aided by the increased defect density and a local rise in temperature (at Al and Mg interfaces). The combination of these effects would permit sufficient diffusion to occur in the interfacial regions of the nanocrystalline grains to form solid solutions [20].

It is worthy to mention that, Al–Mg matrix is more brittle than pure Al due to the presence of Mg atoms and solid solution hardening, which accelerates the fracturing phenomenon and the mechanical milling stages (Figs. 1 and 2).

3.2. Microstructure

Fig. 3 shows X-ray diffraction patterns of Al–10Mg/5Al_2O_3 powder mixtures for different milling times. After 2 h milling all characteristics peaks of FCC aluminum, HCP magnesium and Al_2O_3 are observable in the XRD patterns. With increasing the milling time to 10 h the Al_2O_3 lines disappear due to the reduction of alumina particles to submicron sizes and/or the low volume fraction of the Al_2O_3 phase [16,21]. Also Mg peaks disappeared completely, which indicates the formation of the FCC supersaturated solid solution of Al–Mg ($Al(Mg)_{ss}$)due to the diffusion of Mg atoms into the Al lattice. This was inferred by the clear shift of the Al peaks toward lower angles (Fig. 3(b)), due to the solution of the larger Mg atoms into the Al matrix. Moreover, neither the presence of Al–Mg intermetallics nor unalloyed Mg was revealed from the diffraction pattern, which suggests completed solid solution formation. The results were in good agreement with previous findings [9–12], in which only Al–Mg solid solution was present in alloys up to 30 at.% Mg.

Further milling to 20 h leads to broadening of the $Al(Mg)_{ss}$ peaks and decreasing of their intensities, which indicate reduction in crystallite size and accumulation of heterogeneous strain in the materials. Fig. 4 shows plot of $\beta_s \cos\theta$ versus $\sin\theta$ for Al–10Mg/5Al_2O_3 system milled to 20 h. It was used to calculate the crystallite size and the lattice strain from XRD data [19]. The peak broadening due to crystallite size and lattice strain increases rapidly with increasing θ, but the separation between these two is clearer at smaller θ values. Therefore, it is desirable to use peaks at smaller diffraction angles to separate these two effects [19]. Thus crystallite size was determined using 3 small angle peaks {(1 1 1), (2 0 0) and (2 2 0)} in order to increase the precision of the measurements.

The effect of milling time on the crystallite size and the lattice strain of composite powders is presented in Fig. 5. Up to 10 h, the crystallite size decreases rapidly to about 52 and 34 nm for Al/5Al_2O_3 and Al–10Mg/5Al_2O_3 composites respectively and from 10 to 20 h grain refinement occurs slowly. Plastic deformation of powder particles during milling leads to the increase of crystal defects such as point defects and dislocations [19,22]. The defects increase lattice strain and its internal energy and therefore it becomes unstable. The dislocations rearrange themselves to a lower energy state leading to the formation of low angle sub-boundaries. At longer times of milling and therefore, higher plastic deformation and generation of more dislocations, the misorientations between subgrains at their boundaries increase and eventually they turn into high angle boundaries and become grains with nano-scale sizes [22,23]. Moreover for each milling time, the crystallite size for Al–Mg matrix was lower than for Al. It can be due to the formation of Al–Mg solid solution with higher work hardening effect than pure Al which leads to the trend of crystallite size reduction during milling and facilitation of nanostructure formation.

Generally, the decrease in the crystallite size with milling time is attributed to dislocation generation caused by severe plastic deformation [20,24]. Also in Al–Mg systems, it is found that the Mg concentration has a strong effect on the defect structure. With increasing nominal Mg content of the powder mixture the dislocation density increases [6].

Additionally, up to 10 h the lattice strains increase rapidly to about 0.4 and 0.66% for Al and Al–Mg matrix, respectively (Fig. 5). It may be caused by the introduction of dislocations, vacancies, impurities and other lattice defects during milling [20]. Further milling to 20 h had no observable effect on micro strain level. Also for each milling time the micro-strain of alloyed matrix was higher than pure Al due to the presence of Mg. with diffusion of Mg atoms in Al lattice, interaction of these atoms with dislocations during milling leads to increase in dislocation density [6] and subsequently strain accumulation in particles.

As shown in Fig. 6 lattice parameter increases rapidly for Al–Mg system due to introduction of bigger Mg atoms into Al lattice [6,8,20] and grain refinement [2,25–28]. Generally, the lattice parameter dependence on grain size can be explained as below:

With decreasing the grain size, the volume fraction of grain boundaries increases. It results in some pressure on the interfaces and some tensile stress on the lattice. This consequently can lead to an increase in lattice parameter [25,29].

Also unalloyed matrix shows slight increase in lattice parameter due to grain refinement during milling.

3.3. Microhardness measurements

The profound high hardness of composite powders produced by mechanical alloying method may be due to: work-hardening effect

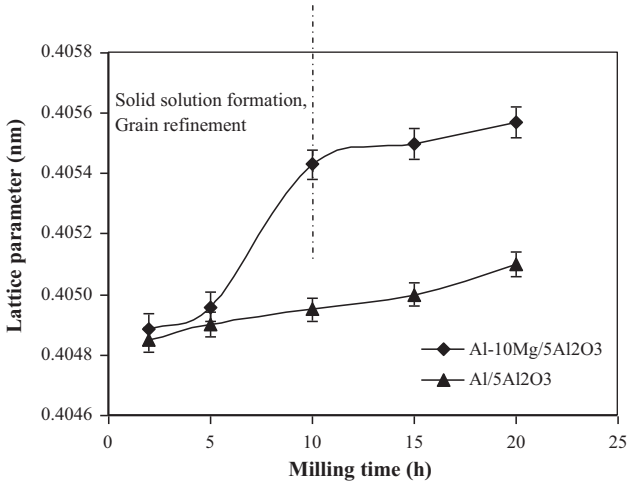

Fig. 6. Evolution of the lattice parameter for $Al/5Al_2O_3$ and $Al–10Mg/5Al_2O_3$ powder mixtures on several milling times.

of the milling operation, the effect of reinforcing phase [15,17] and nano-structure alloy with higher dissolved alloying element much higher than equilibrium content [28].

Fig. 7 shows microhardness changes against milling time. In the $Al/5Al_2O_3$composite after 20 h, microhardness increases to about 118 HV, due to the effect of reinforcing particles [15,17,30], grain size refinement and accumulation of micro-strains [15]. Milling operation leads to fracturing of big brittle alumina particles and more homogeneous distribution of fine brittle powders in ductile Al matrix, which provides local high distortion and work-hardening effects on matrix. Additionally, work hardening effects increase due to plastic deformation of pure Al during milling, subsequently hardness values continues to increase.

Also the hardness (H) can be calculated from the maximum load (F_m) and the maximum penetration depth (h_m) of the indentation curves by the following equation [6]:

$$H = \frac{0.03784 \times F_m}{h_m^2} \quad (3)$$

Up to 10 h, for $Al–10Mg/5Al_2O_3$ composite microhardness increases rapidly to 155 HV and at longer milling times the increasing trend continues with a slower rate (162 HV for 20 h). A distinct difference between microhardness values of Al and Al–Mg matrix can be due to solid solution hardening [6,28,31]. Moreover, Al–Mg

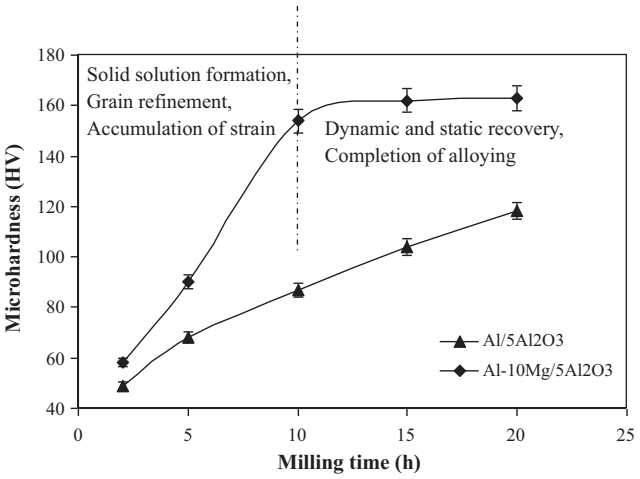

Fig. 7. Variation of microhardness as a function of milling time for $Al/5Al_2O_3$ and $Al–10Mg/5Al_2O_3$ powder mixtures.

solid solution with higher work hardening effect than pure Al leads to the trend of crystallite size reduction [6,20,28] during milling which results in more increase in microhardness compared to unalloyed matrix. From 10 to 20 h, slower rate of increasing in microhardness may be attributed to the completion of alloying process and dynamic recovery caused by high work hardening effects of deformed matrix. It can be also ascribed to static recovery of highly deformed matrix with local increase of temperature in particles during collisions.

Generally, the strength of nanocrystalline solid solutions depends upon both solid-solution hardening and grain-boundary hardening, while the latter makes the major contribution to the total strength. The increase or decrease in hardness is dependent on the combined effects of the hardness increase resulting from solid-solution hardening and the hardness increase or decrease resulting from the changes in grain size and therefore grain-boundary hardening. That is, if solute additions result in a smaller grain size the total effect is hardening, while if they increase the grain size, the result is softening [28].

4. Conclusions

The microstructure and microhardness changes of $Al/5Al_2O_3$and $Al–10Mg/5Al_2O_3$ nanocomposite during mechanical milling were studied. From this study the following conclusions could be drawn:

(1) Steady-state situation occurred in $Al–10Mg/Al_2O_3$ nanocomposite after 20 h milling, due to solution of Mg in the Al matrix, which accelerates the mechanical milling stages, while the situation was not observed in $Al/5Al_2O_3$ nanocomposite after 20 h.
(2) For the binary Al–Mg matrix, alloying process completed after 10 h milling and the predominant phase was an Al–Mg solid solution.
(3) By milling for 10 h, decreasing in the crystallite size (to 52 nm for Al and 34 nm for Al–Mg) and increasing in the lattice strain (to 0.4% for Al and 0.66% for Al–Mg) due to the dislocation generation are observed. On the other hand, profound effect of Mg on these variations is because of diffusion of Mg atoms in Al lattice and formation of AlMg-solid solution which causes generation of more dislocations.
(4) With increasing milling time, the lattice parameter increases slightly for Al matrix while for Al–Mg matrix increases rapidly due to simultaneous effects of solid solution formation and grain refinement.
(5) In the $Al/5Al_2O_3$ composite after 20 h, microhardness increases to about 118 HV, due to the effect of reinforcing particles, grain size refinement and accumulation of micro-strains. On the other hand, for each time higher microhardness values of $Al–10Mg/5\ Al_2O_3$ composite can be due to solid solution formation. From 10 to 20 h, slower rate of increasing in microhardness may be attributed to the completion of alloying process and dynamic recovery caused by high work hardening effects of deformed matrix. It can be also ascribed to static recovery of highly deformed matrix with local increase of temperature in particles during collisions.

Acknowledgment

Authors appreciate the support of the Research Center for Mineral Industries in Shahid Bahonar University of Kerman during the present work.

References

[1] M.S. El-Eskandarani, Mechanical Alloying for Fabrication ofAdvanced Engineering Materials, William Andrew, 2001, p. 2.

[2] M. Delshad Chermahinia, H. Shokrollahi, J. Alloys Compd. 480 (2009) 161–166.
[3] K.D. Woo, H.B. Lee, Mater. Sci. Eng. A 449–451 (2007) 829–832.
[4] N. Al-Aqeeli, G. Mendoza-Suarez, C. Suryanarayana, R.A.L. Drew, Mater. Sci. Eng. A 480 (2008) 392–396.
[5] N. Al-Aqeeli, G. Mendoza-Suarez, A. Labrie, R.A.L. Drew, J. Alloys Compd. 400 (2005) 96–99.
[6] J. Gubicza, M. Kassem, G. Ribarik, T. Ungar, Mater. Sci. Eng. A 372 (2004) 115–122.
[7] S.M. Umbrajkar, M. Schoenitz, S.R. Jones, E.L. Dreizin, J. Alloys Compd. 402 (2005) 70–77.
[8] K.M. Youssef, R.O. Scattergood, K.L. Murty, C.C. Koch, Scripta Mater. 54 (2006) 251–256.
[9] S. Scudino, M. Sakaliyska, K.B. Surreddi, J. Eckert, J. Alloys Compd. 483 (2009) 2–7.
[10] J.C. Crivello, T. Nobuki, T. Kuji, Intermetallics 15 (2007) 1432–1437.
[11] D. Hamana, L. Baziz, M. Bouchear, Mater. Chem. Phys. 84 (2004) 112–119.
[12] D. Singh, C. Suryanarayana, L. Mertus, R.-H. Chen, Intermetallics 11 (2003) 373–376.
[13] T.B. Massalski, Binary Alloy Phase Diagrams, ASM International, 1991, p. 170.
[14] J.B. Fogagnolo, E.M. Ruiz-Navas, M.H. Robert, J.M. Torralba, Mater. Sci. Eng. A 355 (2003) 50–55.
[15] J.B. Fogagnolo, M.H. Robert, J.M. Torralba, Mater. Sci. Eng. A 426 (2006) 85–94.
[16] B. Prabhu, C. Suryanarayana, L. An, R. Vaidyanathan, Mater. Sci. Eng. A 425 (2006) 192–200.
[17] J.B. Fogagnolo, F. Velasco, M.H. Robert, J.M. Torralba, Mater. Sci. Eng. A 342 (2003) 131–143.
[18] G.K. Williamson, W.H. Hall, Acta Metall. 1 (1953) 22–31.
[19] C. Suryanarayana, M. Gerant Norton, X-Ray Diffraction: A Practical Approach, Plenum, New York, 1998.
[20] C. Suryanarayana, Prog. Mater. Sci. 46 (2001) 1–184.
[21] Lidong Zhao, Zwick Jochen, Erich Lugscheider, Surf. Coat. Technol. 168 (2003) 179–185.
[22] Y. Saberi, S.M. Zebarjadb, G.H. Akbari, J. Alloys Compd. 484 (2009) 637–640.
[23] F.L. Zhang, C.Y. Wangb, M. Zhu, Scripta Mater. 49 (2003) 1123–1128.
[24] J.R. Ares, F. Cuevas, Acta Mater. 53 (2005) 2157–2167.
[25] M. DelshadChermahinia, S. Sharafia, H. Shokrollahi, M. Zandrahimia, A. Shafyei, J. Alloys Compd. 484 (2009) 54–58.
[26] M. DelshadChermahinia, M. Zandrahimia, H. Shokrollahi, S. Sharafia, J. Alloys Compd. 477 (2009) 45–50.
[27] M. DelshadChermahini, M. Zandrahimi, M.H. Mirbeik, J. Magn. Magn. Mater. 323 (2011).
[28] C.C. Koch, I.A. Ovidko, S. Seal, S. Veprek, Structural Nanocrystalline Materials: Fundamentals and Applications, Cambridge University Press, New York, 2007, p. 141.
[29] A. William Goddard, W. Donald Brenner, Handbook of Nanoscience Engineering and Technology, CRC Press, 2003, 590-630.
[30] Ismail Ozdemir, Sascha Ahrens, Silke Mucklich, Bernhard Wielage, J. Mater. Process. Technol. 205 (2008) 111–118.
[31] A.A. Mazilkin, B.B. Straumal, E. Rabkin, B. Baretzky, S. Enders, S.G. Protasova, O.A. Kogtenkova, R.Z. Valiev, Acta Mater. 54 (2006) 3933–3939.